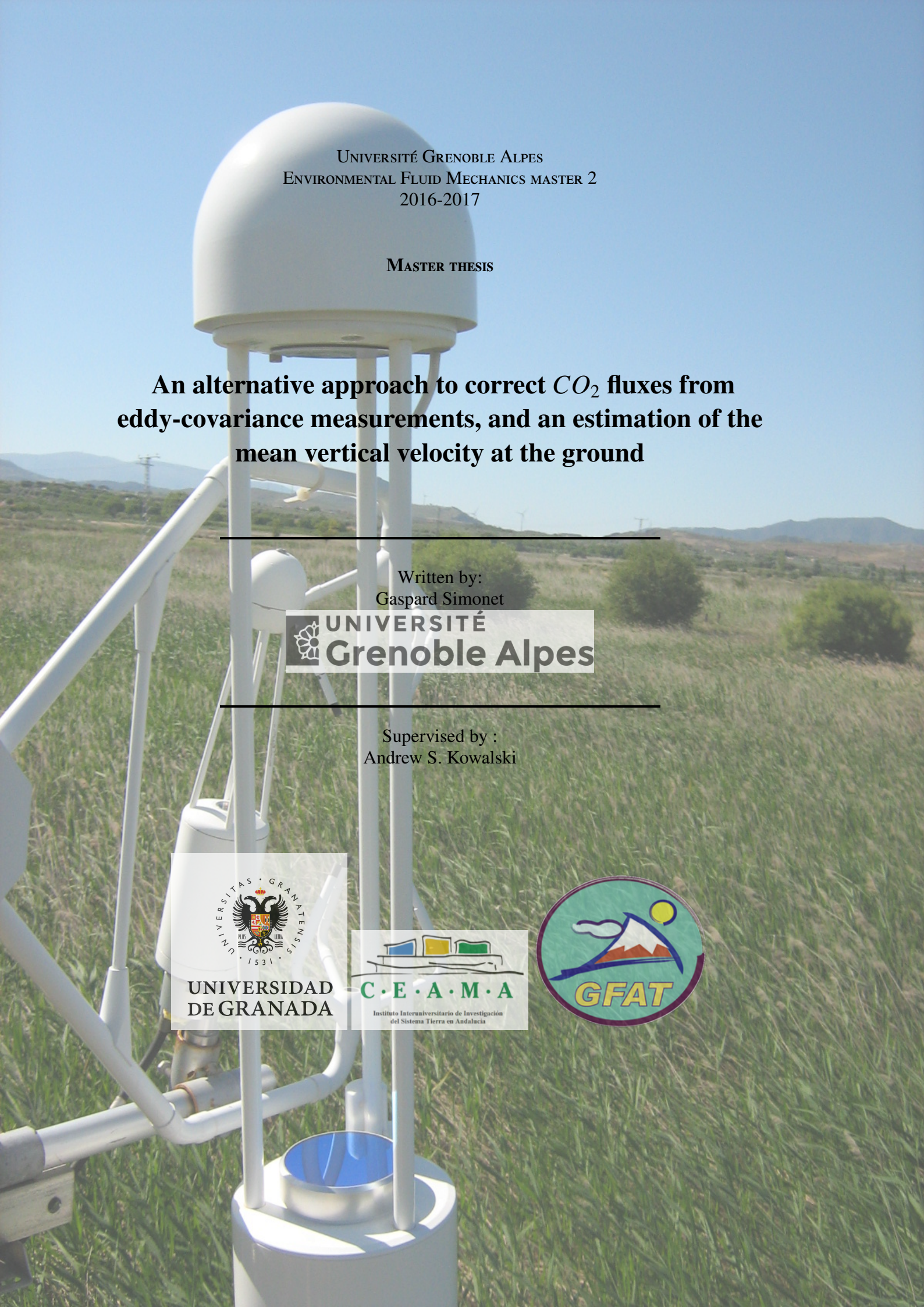

Université Grenoble Alpes
Environmental Fluid Mechanics master 2
2016-2017

Master thesis

An alternative approach to correct CO_2 fluxes from eddy-covariance measurements, and an estimation of the mean vertical velocity at the ground

Written by:
Gaspard Simonet

Supervised by :
Andrew S. Kowalski

Abstract

Wetlands are considered as important sinks of carbon, and accurate estimations of their exchanges are essential for global warming modeling. The objective of this work is to estimate carbon dioxide (CO_2) fluxes over a wetland using two approaches. In this regard, the eddy covariance technique is worldwide used to directly measure CO2 exchanges. However, the implications of mean vertical velocity in calculating gas exchanges is still under discussion. The new method for compute flux of CO_2 (F_{CO2}) is derived from Stefan flow and compared with Webb, Pearman and Leaning (WPL, Webb et al.1980) corrected CO_2 flux. The experimental site is a wetland situated in Padul, southern Spain, where a micro meteorological station records basic quantities at 10 hz since 2012. This station was selected due to the large exchange of matter fluxes occurring over the year and where horizontal homogeneity and no slope under study site are assumed. WPL theory estimates that for an open path *InfraRed Gas Analyzer* (IRGA) the CO_2 fluxes need to be corrected to take account of air density fluctuations. A Matlab© script has been developed to treat the data and to compute these fluxes. As a result, a difference of around -15 $gC.m^{-2}year^{-1}$ of annual average flux was observed between the WPL corrected flux and the flux of this study. Mean vertical velocities at the ground, for these two fluxes, are not defined equally. The WPL velocity appear to be one order greater than Stefan flow velocity, which varies from -0.01 to 0.18 $mm.s^{-1}$, and both are linked with the bowen ratio (β). For a high bowen ratio ($\beta > 5$) the highest WPL velocities are found and for $\beta \simeq 0$ the highest Stefan velocities.

Contents

Chapter 1

Introduction and objectives

Since the dawn of the industrial era, the warming tendency of the atmosphere is known as global warming. This global warming preoccupies many of researchers, in climate sciences, all around the world. In order to improve general knowledges, in 1988, the *Intergovernmental Panel on Climate Change* (IPCC) was created.

The IPCC comprises more than thousands expert researchers who collaborate to establish a robust state of the art on climate change. The knowledge accumulated is organized in assessments and, as times goes by, the level of confidence regarding anthropic implication in the global warming has become very high, from the first to the fifth assessment; (IPCC, 2013). Therefore, in 1992 at Rio de Janeiro (Brazil) the first convention of united states on climate change was written. This convention entered into force in 1994. In 1997, during the *Conference Of Parties* (COP) at Kyoto, Japan, the first protocol aimed to mitigate anthropic emission of *Green House Gases* (GHG) was adopted.

The GHGs are classified into two groups: the well mixed gases such as carbon dioxide (CO_2) and methane (CH_4) which, due to long life times, can be homogenized into the whole atmosphere; and the short lives gases as *Hydrofluorocarbons* (HFC), *Nitrous oxide* (N_2O), *Sulfur hexafluoride* (SF_6) and *Perfluorinated Chemicals* (PFC) which, due to a short time into atmosphere, are not homogenized into the whole atmosphere. These gases, by absorbing and re-emitting a part of total earth radiation -the sum of reflected and emitted part- to the earth's surface, are responsible for global warming of low troposphere. In the COP of Paris, France (2015), a convention was signed to limit the global warming inferior at +2 °C.

The Green House Effect is directly associated with the principle of energy balance: the total energy introduced in earth's system, by solar radiations, should be equal to the sum of fluxes going out of the earth's system. If the budget is not balanced, the lack or the surplus of energy would lead to, respectively, a decreasing or an increasing of the global temperature. The emissions of carbon dioxide can be divided into two categories: the natural emission (volcanoes, wild fire, animals breathing,...) and anthropic (fuel combustion, cement and chemicals production,...). The part of the CO_2 anthropic emission is estimated as 90%, (EEA 2014). In climatology, the emissions are also called "sources" and phenomenas which decrease atmospheric carbon dioxide concentration are called "sinks". Plant respiration and ocean uptake are example of sinks. Since there is a large disparity in the phenomena and repartitions of sources/sinks, it is crucial to accurately assess, by in-situ measurement, the contribution part of each of them.

At the moment, the best method to evaluate the exchanges of mass (gases) or energy, at the ecosystem scales - from μm to km in space and second to year in time- is called the *Eddy Covariance* technique (EC). It involves installing, over the surface studied, a micro-meteorological tower. The height of the tower can varies from meter to hundreds of meter for the highest and determines the footprint size -the area measured by instruments- and the size of eddies -associated with turbulent movements- which can be measured. This technique, by providing a high frequency measurement, gives direct information of fluxes in the time range of half-hours to years. That is

why a global network of long-term eddy-covariances fluxes (energy and GHG fluxes) is expanding. Currently, FLUXNET provides a database of micro-meteorological towers, for close to 850 sites, in all continents.

The EC technique is subjected to "the energy balance closure". This issue comes from the fact the balance in input energy is not equal at the ouptut energy in the measurement point, this balance can be written as (Wilson and al. 2002):

$$H + LE = R_n - G - S - Q \tag{1.1}$$

where R_n is the net radiation; H and LE, respectively, the turbulent sensible and latent heat fluxes; G the heat flux into the soil substrate; S the rate of change of heat storage between soil and measurement height and Q represents all additional sources/sinks of energy. The closure problem is that, in the eq.1.1, left-hand-side equation does not equal the right-hand-side, and the ratio of both is, closely, equal to 0.8.

The difficulty of modeling the energy balance comes from the large disparity in space and time of the different terms in eq 1.1 and their approximations. After 20 years of scientists' community attempting to solve this problem, the mains errors come from both: the measurement techniques and the error estimations (Foken, 2008).

Additionally, the vertical velocity in surface layer stays a key variable in atmospheric sciences. As a matter of fact, this velocity defines the turbulent heat fluxes H and LE. Since this velocity is very tiny in comparison of the sensor's precision, a good estimation is, therefore, of a primordial importance.

This study aims to compare two methods of CO_2 exchange fluxes estimation for open path gas analyzers in the wetland of Padul, southern Spain. The Millennium-Ecosystem-Assessment (MEA.2005), estimates that wetlands cover about 3% of earth's land surface and are considered as a global sinks of atmospheric CO_2 and storing pool of around 28% of global soil carbon. This very large implication of wetlands into the carbon earth balance implies a need to understand and to estimate correctly the phenomenas occurring in such places.

The first method is well known as WPL corrected CO_2 flux and the second method is a new method using variables weighted with density factor and an other definition of mean vertical velocity at the ground, derived from Stefan mass flow.

In order to introduce more specifically the work done during this internship, some physical considerations are recalled and/or developed, then the methods of processing data will be presented. After that, the main results will be given and discussed.

Chapter 2

State of the art

All phenomena and considerations presented in this study have been studied in the context of *Planetary Boundary Layer* (PBL) and more specifically in the *Surface Layer* (SL). The PBL is defined as "the part of the troposphere that is directly influenced by the presence of the earth's surface, and responds to surface forcings with a timescale of about hour or less" (Stull, 1988). The SL is the lowest 10% of the PBL just above the ground. It is also important to introduce the notion of *turbulence* which is strongly present in the SL. Currently, turbulence has not a scientific consensus for its definition. Nevertheless, turbulence phenomena can be described as:

- ◇ Random and unpredictable: As chaos theory and Lorenz attractor examples, even with a quasi-infinite precision in the initial conditions, flows are not descriptive in a deterministic way. Statistical description, then, remains the most suitable way to describe turbulence.
- ◇ Non-linear effects: the turbulence properties are mainly controlled by the non-linear terms in the governing equations. The Reynolds number Re permits identifying the state of the flow by comparing, as a ratio, non-linear effect with linear effect. Over a critical value Re_C, the flows is considered as turbulent and, in environmental conditions, this state is very common.
- ◇ Transport and mixing: in the form of eddies, turbulence enhances transport and mixing. Depending on the size, and the frequency in time, these phenomena are very important to take account in association with molecular diffusion and non-diffusive transport.
- ◇ Multi-scale: a continuous spectrum of scales is a very important characteristic of turbulence. For example the mean wind for a micro-meteorological scale can be considered as turbulence at the synoptic scale. This implies the need to well specify the scales at which observations are realized.

2.1 Reynolds decomposition

In 1895, Osborne Reynolds has introduced, in the paper "On the Dynamical Theory of Incompressible Viscous Fluids.." (Reynolds, 1895), the notion of averaging of field variables. It is well known as "Reynolds Averaging" and this averaging allows scientists to distinguish a "mean part" of a quantity ϕ with its "fluctuation part" ϕ', which is very often also called "turbulent part", finally the "instantaneous" part is expressed as:

$$\phi = \bar{\phi} + \phi' \tag{2.1}$$

This decomposition implies to look at the scale, either in time and in space, at which we are studying because of an interval needing to average. This interval will be equivalent to an high-pass filter of turbulence longer than this intervals, (Lee et al. 2004). The definition of averaging are

specified in the next subsection, but, this notion is called "block-averaging" because we decompose the signal into N blocks of equal size. In this study, all furthers definitions and utilizations of averaging will underlie this property of averaging with block size (time-period) of half hours, as is most common in micro-meteorology, (Finnigan et al. 2003).

2.2 Averaging methods

By definition, there are three kinds of averages: time averages, spatial averages and ensemble averages. Time average consists of integrating a variable over time whereas the spatial average consist to integrate the variable over space dimensions (line, area, volume). The ensemble average is, generally, more suitable for experiments because it involves to sum over a number of experiments, (Stull. 1988). Note that regarding quantity definitions, sensor's records, even at high frequency , are already averaging. For example, the temperature is defined as the average molecular kinetic energy. Considering homogeneous and stationary turbulences between two measurement, t and $t + 1$ for time or x and $x + 1$ for space, it is possible to define the generic average (eq. 2.2), this average comes from the ergodic conditions which states that the three averages are equal.

2.2.1 Generic average

This type of averaging is the most used in micro-meteorology. Since it is the most convenient to recording data, this average actually corresponds to a time average. Currently, most of the sensors of meteorology record over time at 10 Hz corresponding to 10 measurements each seconds. Then if we consider N measurement, over a time t, the generic average is expressed as:

$$\bar{\phi}_t = \frac{1}{N} \sum_{i}^{N} \phi_i \tag{2.2}$$

where ϕ is a quantity (vectorial or scalar) and the index i indicates the number of measurement.

2.2.2 Weighted average

Some authors (Hesselberg. 1926, Kramm. 1995, Kowalski. 2012) have shown that for air temperature, mixing ratio and velocity a weighting factor is necessary to more accurately take account the effect of density variations in the averaging of these intensive quantities. Following the previous notation, ϕ describes any meteorological variables, $\widetilde{\phi}$ the averaged part and ϕ'' the fluctuation part. As the equation 2.1, we express the instantaneous part as:

$$\phi = \widetilde{\phi} + \phi'' \tag{2.3}$$

And the weighted average is defined as:

$$\widetilde{\phi} = \frac{\frac{1}{N} \sum_i^N (\phi_i \alpha_i)}{\bar{\alpha}} = \frac{\frac{1}{N} \sum_i^N (\phi_i \alpha_i)}{\frac{1}{N} \sum_i^N \alpha_i} \tag{2.4}$$

where α is the appropriate weighting factor, (Kowalski. 2012).

This average follows the same rules of Reynolds' rules, see appendix A of Kramm, 1995:

$$\begin{aligned}
\overline{c} = \widetilde{c} = constant \qquad \overline{A'} = \widetilde{A''} = 0 \\
\overline{(cA)} = c\bar{A} \qquad \widetilde{(cA)} = c\widetilde{A} \\
\overline{(\bar{A})} = \bar{A} \qquad \widetilde{(\widetilde{A})} = \widetilde{A} \\
\overline{(\bar{A}B)} = \bar{A}\bar{B} \qquad \widetilde{(\widetilde{A}B)} = \widetilde{A}\,\widetilde{B} \\
\overline{(A+B)} = \bar{A} + \bar{B} \qquad \widetilde{(A+B)} = \widetilde{A} + \widetilde{B} \\
\overline{\left(\frac{dA}{dt}\right)} = \frac{d\bar{A}}{dt} \qquad \widetilde{\left(\frac{dA}{dt}\right)} = \frac{d\widetilde{A}}{dt} \\
\overline{(A.B)} = \bar{A}\,\bar{B} + \overline{(A'B')} \qquad \widetilde{(A.B)} = \widetilde{A}\,\widetilde{B} + \widetilde{(A''B'')}
\end{aligned} \tag{2.5}$$

With A and B any scalar or vectorial quantity.

2.3 CO_2 fluxes

Following the fundamentals laws and applying the Reynolds' decomposition (eq. 2.5), the pollutant fluxes are defined as the covariance between the density of the pollutant specie and the vertical velocity as :

$$F_{co2} = \overline{\rho_{co2} w} = \overline{\rho'_{co2} w'} + \overline{w}\,\overline{\rho_{co2}} \tag{2.6}$$

where ρ_{co2} is the density of carbon dioxide in $Kg.m^{-3}$ and w' the turbulent part of vertical velocity in $m.s^{-1}$. A very classical assumption (Burda, Anderson. 2010) is to neglect the mean vertical flow, or considering the vertical velocity equals zero, and let eq.2.6 as:

$$F_{co2} = \overline{\rho'_{co2} w'} \tag{2.7}$$

2.4 WPL correction

Webb, Pearman and Leening in 1980 have shown that the fluxes of trace gas species, when measured by open-path gas analyzers, need corrections to take account of the change of CO_2 density. These density changes occur due to three main effects: the photosynthesis and respiration reactions, the evaporation of water and the dilatation/compression of the control volume. The photosynthesis, by uptaking CO_2 during the day and the respiration releasing it during the night, leads to an increase and a decrease in ρ_{co2} during, respectively, night time and day time. The *Evapo-Transpiration* (ET) or also called turbulent latent heat flux (LE), by adding water gas molecules into the control volume, will reduce the space "available" for other species in the volume. This effect leads to a decreasing of CO_2 density. The compression/dilation of the volume is controlled by the turbulent sensible heat flux (H). This flux leads to changes of temperature of the control volume and, at constant pressure, following the ideal gas law $P = \rho RT$ leads to decreasing of ρ_{co2} with increasing of T.
Using $\sigma_{co2} = \overline{\rho_{co2}}/\overline{\rho_a}$, $\sigma_v = \overline{\rho_v}/\overline{\rho_a}$ and $\mu = Ma/Mv$ which is the ratio of molecular of dry air and water vapor, the correction is usually expressed as:

$$F_{co2} = \overline{\rho'_{co2} w'} + \mu\sigma_{co2}\overline{\rho'_v w'} + \overline{\rho_{co2}}(1 + \mu\sigma_v)\frac{\overline{w'T'}}{\overline{T}} \tag{2.8}$$

with ρ_{co2} the density of CO_2 gas, ρ_v the water vapor density, T the temperature and w the vertical velocity. Writing in term of turbulent latent heat flux $LE = L_V\overline{\rho'_v w'}$ and in term of turbulent

sensible heat flux $H = \rho C_p \overline{w'T'}$, where C_P and L_V are, respectively, the specific heat of moist air and the latent heat of vaporisation, eq. 2.8 becomes:

$$F_{co2} = \underbrace{\overline{\rho_{co2} w'}}_{Raw\ flux} + \underbrace{\frac{\mu \sigma_{co2} LE}{\rho L_V}}_{Latent\ Heat\ correction} + \underbrace{\overline{\rho_{co2}}(1 + \mu\sigma_v)\frac{H}{\rho \overline{T} C_p}}_{Sensible\ Heat\ correction} \tag{2.9}$$

Expressing the specific humidity as $q = \rho_v/\rho$, the mean vertical wind component, from WPL correction, is defined as:

$$\overline{w}_{WPL} = \frac{\overline{w'T'}}{\overline{T}} + \overline{w'q'} \tag{2.10}$$

Or, to observe relative importance of H and LE, eq.2.10 could be written as, eq.10 Kramm et al. 1995:

$$\overline{w}_{WPL} = \frac{H}{C_P \overline{\rho}} \left(\frac{1}{\overline{T}} + \frac{C_P}{\beta L_V} \right) \tag{2.11}$$

where $\beta = H/LE$ is the Bowen ratio which quantified the relative importance of the sensible heat flux with respect to the latent heat flux.

2.5 Diffusive part and Stefan flow

A vertical velocity can be extracted, from gas exchanges, through the law of conservation of linear momentum (Finnigan, 2009):

$$w = \frac{\sum_{i=1}^{N} w_i \rho_i}{\rho} \tag{2.12}$$

where the index i denotes a gas species. For the atmosphere, i could takes the values of *nitrogen gas* (N_2), *dioxygen* (O_2), *argon gas* (Ar), *carbon dioxide* (CO_2) and water vapor (H_2O) which are the species the most present in our atmosphere. The eq.2.12 can be written as:

$$w\rho = w_{(N_2)}\rho_{(N_2)} + w_{(Ar)}\rho_{(Ar)} + w_{(O_2)}\rho_{(O_2)} + w_{(CO_2)}\rho_{(CO_2)} + w_{(H_2O)}\rho_{(H_2O)} \tag{2.13}$$

where the last term, $w_{(H_2O)}\rho_{(H_2O)}$, is dominant in r.h.s. and permits to neglect other terms, leading to:

$$w_{Stefan} = \frac{w_{(H_2O)}\rho_{(H_2O)}}{\rho} = \frac{E}{\rho} \tag{2.14}$$

which describes the velocity of Stefan flow.

The Stefan flow describes a net non-turbulent upward flow, with a mean vertical velocity normal to the surface, where evaporation takes place, (Bird et al. 2002).

This average velocity is induced by water evaporation and transport scalar (mass of CO_2 in our study), in non turbulent transport, as following (Kowalski, 2017):

$$F_{CO_2,ND} = w_{Stefan} \times \rho_{c,i} \tag{2.15}$$

An other part of the transport of mass is accomplished by turbulences, trough eddy diffusivity, that we call "diffusive" part. The diffusive part of CO_2 flux is calculated using the turbulent part of CO_2 mass fraction:

$$F_{CO_2,DIF} = \overline{w'' f''} \rho \tag{2.16}$$

Note that the mass fraction, $f = m_{CO_2}/m_{air}$ is used instead of the CO_2 density, the mixing ratio ($c = m_{CO_2}/m_{dry\ air}$) and the molar fraction ($\chi = n_{CO_2}/n_{air}$), (Kowalski, Serrano-Ortiz. 2007).

Finally, the CO_2 flux of this study is composed of the sum of the diffusive and non-diffusive part as:

$$F_{CO_2} = F_{CO_2,DIF} + F_{CO_2,ND} = \overline{w'' f''} \rho + w_{Stefan} \times \rho_{c,i} \tag{2.17}$$

Chapter 3

Material and methods

3.1 Experimental site: the wetland of Padul

The wetland of Padul is located at the bottom of the Sierra Nevada mountains, at *El Padul* in the province of Granada, southern Spain, and so on in the Sierra Nevada National Park (see fig.3.1) in the Lecrin valley. This station is Called "ES-pdu" in the European fluxes Database cluster.

More precisely, the measurement station is found at the coordinates 37°00′ N 03°36′ O and at an altitude of 744m. This experimental site was installed in June 2012 and, at the moment, it is still operating.

The surface of this wetland is estimated at 3.3 Km^2 (Serrano-Ortiz et al. 2017) and the tower footprint, which is the estimation of surface measured by tower's instruments, is close to 0.50 Km^2, see fig 3.1. By definition, wetlands are areas which are covered by water during varying periods and therefore develop special vegetation. Padul's wetland is considered as a sub-humid wetland, and so is subjected to inconsistent rainfall patterns and high temperatures. The wetland of Padul is also classified as "inland" wetland, that means which is not subjected to tidal effect.

The main particularities of this observation site are its flatness and the homogeneity of the species around the tower. Indeed, the site is flooded more than the half of the year (Serrano-Ortiz et al. 2017), and a stagnation of water is observed. The main species which grows at the Padul site is *Phragmites australis*, or the common reed, which has been widely studied (Brix et al.2001) to improve the understanding of their exchange as source/sink of GHG with atmosphere. In addition, large mass fluxes (of H_2O and CO_2) are observed in Padul. The particularity of this valley is the very often windy conditions. These windy conditions ensure turbulence at the ground due to the high Reynolds number and allow us to compute turbulent matter fluxes in accordance to literature of atmospheric boundary layer. What is more, at few km of the study site, wind electrical turbines are installed to provide energy. Theses particularities make of Padul's observation site an ideal place to use the hypothesis of homogeneity, turbulent conditions and quasi no slope terrain in further calculations.

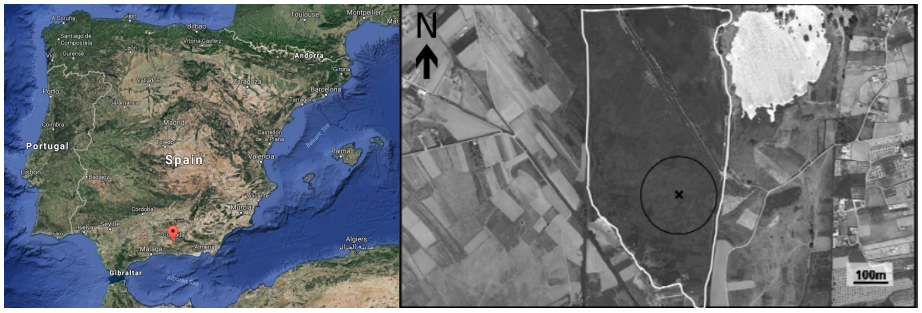

Figure 3.1: Left, localization of Padul with red marker, source Google Earth. Right, photo of Padul's wetland from aircraft. The white solid line indicates the common reed area and the white area at the right top is a lack. The black cross (X) indicates the position of EC tower, the black circle shows the maximum fluxes source location (from Flux-source Area model of Schmid, 1994). Source: "Sistema de Información Geográfica de Parcelas Agrícolas" (SIGPAC) and reproduced from Serrano-Ortiz et al. 2017.

3.2 Measurements

The micro-meteorological station of Padul is equipped with open-path IRGAs (*Infra Red Gas Analyzer*) the LI-7500 (LI-COR inc., Lincoln, NE, USA). They measure, respectively, the CO_2 and H_2O gas densities density 6m above ground level at a response of 10 Hz. A hight frequency sonic anemometer CSAT-3 (CAMPBELL SCIENTIFIC inc., Logan, UT, USA), also at 6m, measures the winds components in 3-directions at a response of 10 Hz. The records of measurements are provided by the data logger CR3000 (CAMPBELL SCIENTIFIC inc., Logan, UT, USA). The table 3.1 summarizes the main characteristics of the measurements.

Table 3.1: Sensors of Padul's micro-meteorological station used in this study. The column "Variables" represents the quantities measured by the different sensor; "Unit" gives the output units of the sensors; "Accuracy" is given in root-mean-square and "Frequency" represents the frequency of sampling.

Sensors (Height [m])	**Variables**	**Unit**	**Accuracy**[1]	**Frequency**
Sonic Csat-3[2] (6m)	U	$m.s^{-1}$	$\pm 1 mm.s^{-1}$ rms	10 hz
	V		$\pm 1 mm.s^{-1}$ rms	
	W		$\pm 0.5 mm.s^{-1}$ rms	
	Temperature	°C	±0.025 °C rms	
IRGA 1: LI-7500[3] (6m)	ρ_{CO2}	$mg.m^{-3}$	$\pm$ 0.19$mg.m^{-3}$ rms	10 hz
	ρ_{H2O}	$g.m^{-3}$	$\pm$ 3.3$mg.m^{-3}$ rms	
	Pressure	KPa		

[1] From constructor specifications in standard conditions T=25°C and P=98 KPa.
[2] CAMPBELL SCIENTIFIC inc. Logan, UT, USA.
[3] LI-COR inc. Lincoln, NE, USA.

3.2.1 Data base

The station of Padul records data since 2012, at 10 Hz frequency. An example of raw data is given in fig. 3.2. In this figure, it is possible to see the date and the time of the measurement, the variables name, the unity of the measurements and finally the columns "diag_csat" and "diag_irga_raw" indicate the state of the sensors. A further discussion concerning these quantities will be held in the next section. The first step to obtain this data is to uncompressed binary files, using the "card-converter" software developed and distributed by Eddy-Pro, of a period between two consecutive site's visits. Eddy pro is currently the free software which is considered as reference in micro-

meteorological eddy covariance computation. During these visits, IRGA sensors are cleaned and data are downloaded from the logger to liberate space for the further measurement data. The logger has a capacity of two months of data storing which corresponds to 4 Gbytes of memory space. For the year of 2015, it corresponds to closely 25 Gbytes of raw data. After that, a bash script was realized to detect and "normalize" the error codes into these data. The error code researched was: "-9999"; "9999"; "INF"; "-INF"; "NAN" to replace with "NaN" value which will be used in the Matlab© processing script.

```
"TOA5","3547","CR3000","3547","CR3000.Std.09","CPU:PAD V1.4.CR3","473","ts_data"
"TIMESTAMP","RECORD","Ux","Uy","Uz","Ts","co2","h2o","press","diag_csat","diag_irga_raw"
"TS","RN","m/s","m/s","m/s","C","mg/m^3","g/m^3","kPa","unitless","unitless"
NaN,NaN,"Smp","Smp","Smp","Smp","Smp","Smp","Smp","Smp","Smp"
"2015-09-01 00:00:00.1",497941957,-1.36875,-3.914,0.0745,25.55899,525.1956,18.40892,92.78443,0,250
"2015-09-01 00:00:00.2",497941958,-1.17,-4.09425,0.1225,25.49689,523.9252,18.34676,92.78443,0,250
"2015-09-01 00:00:00.3",497941959,-1.371,-3.83825,0.24075,25.57104,523.9409,18.37353,92.78443,0,250
"2015-09-01 00:00:00.4",497941960,-1.3845,-3.81875,0.2625,25.40036,524.1433,18.36572,92.78443,0,250
"2015-09-01 00:00:00.5",497941961,-1.53675,-3.7575,0.20175,25.46591,523.485,18.35929,92.78443,0,250
```

Figure 3.2: Example of raw data base once uncompressed.

3.3 Processing methods

This section relates the procedure used in the script development to treat raw data to final results. First, the way of filtering raw data is specified and, secondly, how CO_2 and mean vertical velocities were computed either for the classical WPL correction and for this study.

3.3.1 Pre processing: quality assessment of raw data

The turbulent fluxes transporting either momentum, energy or scalar are strongly dependent on the quality of the sensors. In the case of CO_2 fluxes, we mainly use a high-frequency three-dimensional anemometer and an IRGA. These sensors are subjected to weather events like strong wind, rain, snow and, in the case of Padul station, also rain with sand from Sahara desert. These conditions affect, principally, the IRGA sensor since it is composed of two lenses which measure the density of water and CO_2 trough the Beer-Lambert law of absorption. For example, an underestimation of ρ_{co2} by 5% could lead to a CO_2 flux overestimation of 13% (Serrano-Ortiz et al. 2008). This result shows the importance of using data with good functioning of sensors.

In order to use the data with physical significance, a method of data filtering was implemented into the code. In literature, a wide variety of methods was developed to estimate the quality of high frequency data. Usually they are based on (Mauder and al. 2013): High frequency data test; Statistical test on data and fluxes; Quantification of the error/uncertainties estimates.

The complexity, the cost in calculation and the results of such filters can largely vary from the software which is used to an other (Mauder and al. 2008). To avoid a large cost of calculation, due to many iterations, the part of statistical test and the quantification of error/uncertainties estimates was not realized into our script. Indeed, for the fluxes of CO_2 the differentiation permits to not take account the errors on the real values of each fluxes because they are computed with the same filtered data. Nevertheless, this study has tried to follow the strategy of filtering of *TERENO* (TERrestrial ENvironmental Observatories) which is the long-term ecosystem networks in Germany.

Flag of quality of sensors

The first test effected on the raw data was to neglect data measured during malfunctioning of the devices. Indeed, the devices C-sat and LI-7500 are able to attach, for each measurements, a flag of quality attesting the state of the sensors. The values of flags are given in bytes format varying from 0 to 63 and 0 to 255 for, respectively, the C-sat and the LI-7500. Once converted into decimal

numbers, the quality flags indicate the state, functioning or not, of the different sensor's part and a quality/accuracy estimation of the measurement. From the constructor sensor manuals, the best quality of values range from 248 to 250 for the IRGA sensor and is 0 for anemometer sensor. For this study, we made the choice to use only these values.

Table 3.2 compares the range of values used in this study and those used in TERENO. Please note that the criteria of this study, concerning the sensor's quality flag, are more restrictive. At this step, if a value of one sensor did not pass this quality test, others values from the other sensor is flagged as incorrect value. This treatment permits a better estimation of each variables during statistical operations as mean, variance and covariances.

	This study		**Mauder and al. 2013**	
Sensors	Min.	Max.	Min.	Max.
C-sat300 diag.	0	0	0	63
LI-7500 diag.	248	250	240	251

Table 3.2: Comparison of the diagnostic values used in this study and the values used in TERENO (Mauder and al. 2013).

Thresholds

This filtering step consists of keeping only values in plausible physical ranges. Because the sensors quality flags step does not filter the values which have no physical sense, as a temperature of 350 K or a density of water of -6 $g.m^{-3}$, simple absolute limits are fixed to remove this issue. The ranges used in this study are summarized in the table 3.3.

After this step, "block-averaging" of half hours is applied. With a 10 hz frequency response sensor this implies decompose the time series in 18000 values. The block half hour averaging, as presented in the previous chapter, is the reference to distinguish the fluctuation part and mean part of any quantity (scalar or vectorial).

Quantity	**Lower limit**	**Upper Limit**	**Units**
U,V	-30	30	$m.s^{-1}$
W	-10	10	$m.s^{-1}$
Ts	253	323	K
P	90	130	KPa
$[H_2O]$	0	35	$g.m^{-3}$
$[CO_2]$	0.1	3	$g.m^{-3}$

Table 3.3: Absolute limits of quantities used in this study. Where W is vertical wind component, Ts the sonic temperature, P the atmospheric pressure, $[H_2O]$ the density of water vapor and $[CO_2]$ the density of CO_2 gas.

Median Absolute Deviation

Following the method used in Mauder and al.2013, we applied on unique statistical test. This test uses the Median Absolute Deviation (MAD) and permits despiking of statistically outliers from the median as follow:

$$\langle x \rangle - \frac{q.MAD}{0.6745} \leq x_i \leq \langle x \rangle + \frac{q.MAD}{0.6745} \tag{3.1}$$

where $\langle x \rangle$ is the median of the quantity x (for the ith measurement) and MAD is defined as:

$$MAD = \langle |x_i - \langle x \rangle| \rangle \tag{3.2}$$

where q is threshold value, set to 7, and 0.6745 relates to a deviation's factor of Gaussian distribution of quantity x. Please note that a value of q too low will lead to classified as outliers values which was not. The MAD statistical test can be represented as a "window", as in figure 3.3, which is moving in the time series every half hour.

At this step, likewise that the first step, we neglect all the values a the time of measurement t for all variable x_t.

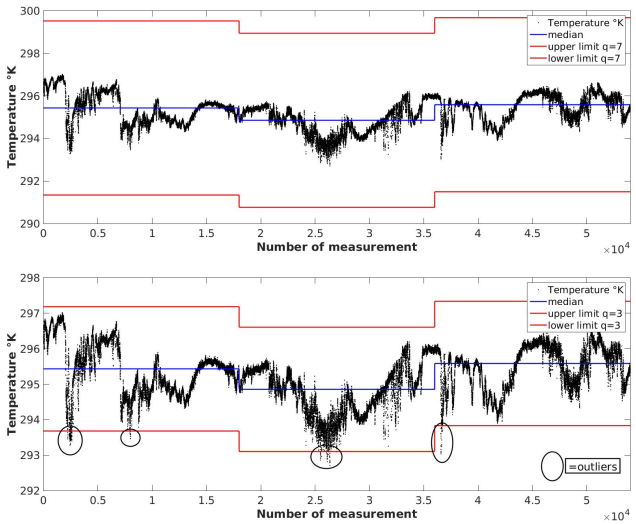

Figure 3.3: Example of moving MAD windows on 3 half hours (54000 values) for, at the top, q=7 and, at the bottom, q=3. The values are plotted in black dot, median in blue line and windows around median in red lines. The ellipsoids represent outliers.

Percentage of bad values

Finally, half hours with more than 180 bad values were rejected, which corresponds to 1% of half hour values. This filter data step is more restrictive than the usual convention which varies from 10 to 30 % for the computing of turbulent fluxes. And once again, if one quantity at the half hours h fails the previous test, all the variables x_h are rejected.

3.3.2 Processing

In this section, a brief description of processing step in the Matlab script is given. After the import of raw data, the change of units into international system units and the pre-processing steps, described in previous section, the partial pressure of water vapor is computed. Using the ideal gas law, the partial pressure of water vapor is:

$$e = \rho_v R_v T_s \tag{3.3}$$

where ρ_v is the measured density of water vapor in $kg.m^{-3}$, R_v is the perfect gas constant for water vapor, took equal to 461.5 $J.Kg^{-1}.K^{-1}$, and T_s the sonic temperature in Kelvin. Dalton's law allows us to express the dry air pressure as:

$$P_{dry} = P - e \tag{3.4}$$

where P is the total pressure measured in-situ in Pa. Then, it is possible to compute the density of dry air as:

$$\rho_d = \frac{P_{dry}}{R_d.T_s} \tag{3.5}$$

where R_d, the dry air gas constant, is equal to 287 $J.Kg^{-1}.K^{-1}$. Finally, we expressed the total density of humid air as:

$$\rho = \rho_v + \rho_{dry} \tag{3.6}$$

At that point, all useful variables are decomposed into half-hour blocks and averaged following the two methods described in equations 2.2 and 2.4. Using ρ as weighting factor for the vertical velocity, ρC_P for the temperature and 1 for the densities.

Once the mean values computed, the turbulent part is "extracted" from measured and averaged part following equations 2.1 and 2.3. At that moment, the H_2O, CO_2 and temperature fluxes are calculated for the two kinds of variable (classical and weighted) as:

$$\begin{aligned} F_{(H_2O)}1 &= \overline{w'\rho'_{v,i}} = \frac{\sum_i^N(\rho'_{v,i}w'_i)}{N} & F_{(H_2O)}2 &= \overline{w''\rho''_{v,i}} = \frac{\sum_i^N(\rho''_{v,i}w''_i)}{N} \\ F_{(CO_2)}1 &= \overline{w'\rho'_c} = \frac{\sum_i^N(\rho'_{c,i}w'_i)}{N} & F_{(CO_2)}2 &= \overline{w''f''}\rho = \frac{\sum_i^N(f''_{c,i}w''_i\rho_i)}{N} \\ F_{(Ts)}1 &= \overline{w'T'_s} = \frac{\sum_i^N(Ts'_iw'_i)}{N} & F_{(Ts)}2 &= \overline{w''T''_s} = \frac{\sum_i^N(Ts''_iw''_i)}{N} \end{aligned} \tag{3.7}$$

Where $N = 18000$ values, which corresponds to measurement of one half-hour. After this step, WPL mean vertical velocity is calculated:

$$Wmean_{(WPL)} = \overline{w} = \frac{F_{(Ts)}1}{\bar{T}_s} + \overline{w'q'} \tag{3.8}$$

where $q = \rho_v/\rho$ is the specific humidity and q' its turbulent part following classic Reynolds decomposition. The CO_2 flux corrected by WPL theory is also calculated at this step using eq. 2.8 and $F_{(H_2O)}1$, $F_{(CO_2)}1$ and $F_{(Ts)}1$. Concerning the Co_2 flux of this study, we write the total water vapor flux as:

$$F_V = F_{V_{diff}} + F_{V_{non-diff}} = F_{V,d} + w\rho_v = F_{V,d} + \frac{F_V\rho_v}{\rho} = F_{V,d} + F_Vq \tag{3.9}$$

So, the total water vapor flux is $F_V = F_{V_{diff}}/(1-q)$. Then the mean vertical velocity, non diffusive, induced by evaporation is computed as:

$$Wmean_{(Stefan)} = Wmean_{ND} = \widetilde{w} = \frac{\frac{F_{(H_2O)}2}{1-q_i}}{\bar{\rho}} \tag{3.10}$$

and the non diffusive part of CO_2 flux as:

$$F_{(CO_2,ND)} = Wmean_{ND} \times \rho_{c,i} \tag{3.11}$$

Finally, the CO_2 flux of this study is the sum of a diffusive part and a non-diffusive part as $F_{CO_2} = F_{CO_2,ND} + F_{CO_2}2$.

Chapter 4

Results

This chapter aims to show the main results of this study. The first section will present the evolution of CO_2 fluxes, from this study and from the WPL theory, for the year of 2015 and how the differences in these fluxes are influenced by the differences in mean vertical velocities ($\widetilde{w}$-$\overline{w}$). After that a second section will present the mean vertical velocities of this study and from WPL theory for their evolution over the course of the year, their diurnal cycle and, as well, the factors which influence them during the year 2015.

The data of the year of 2015 have been selected due to its better data quality in comparison with the others. Note that a technical IRGA problem occurred in the middle of September until the end of October. Therefore, the data for this period are not used. For this year, after filtering raw data, close to 65% of data were used which corresponds to 11526 available half-hour values.

4.1 CO_2 Fluxes

4.1.1 Evolution over the year

Figure 4.1 gives the values of CO_2 fluxes for the computation used in this study and for the classical computation using WPL correction. The values range from -30 to 30 $\mu mol.m^{-2}.s^{-1}$ and the sign convention used is positive for releases into atmosphere and negative for uptake into the surface. For the summer period, May to September, the dispersion of values is greater than for the rest of the year and occupies all the range of possible values. The minimum values are reached during this period of spring and summer, the daily average oscillates between -3 to -10 $\mu mol.m^{-2}.s^{-1}$. During the months of June and July the uptake of CO_2 reaches the maximum for the year. For the other periods of the year, the daily average is close to zero. The average over all values of CO_2 WPL corrected flux is -1.53 $\mu mol.m^{-2}.s^{-1}$ and the average of the flux of this study is -1.57 $\mu mol.m^{-2}.s^{-1}$. In both fluxes, the annual average value of these fluxes are negative.

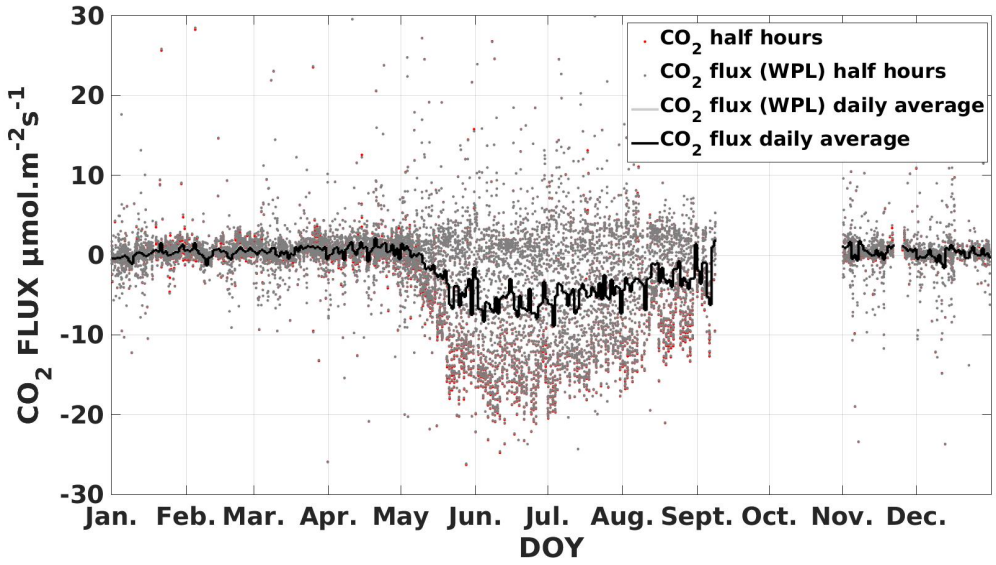

Figure 4.1: Fluxes of CO_2 versus the *Day of year* (DOY), red and black dots represent half hours values. Grey and black lines represent, respectively, daily average values of this study and for the WPL correction. All fluxes are given in $\mu mol.m^{-2}.s^{-1}$.

Since the differences in Fig. 4.1 are not well appreciable visually, the differences between the two computations of CO_2 fluxes are shown in Fig.4.2. From January to May, the differences are more pronounced and range from -0.4 to 0.1 $\mu mol.m^{-2}.s^{-1}$. The second weeks of April, a maximum in the differences between the two fluxes is observed and reaches -0.8$\mu mol.m^{-2}.s^{-1}$. The daily average fluctuates between 0 to -0.2 $\mu mol.m^{-2}.s^{-1}$ for the winter and the spring period, November to May, and is close to zero during summer. The average difference of the two fluxes is -0.04 $\mu mol.m^{-2}.s^{-1}$ during the year of 2015.

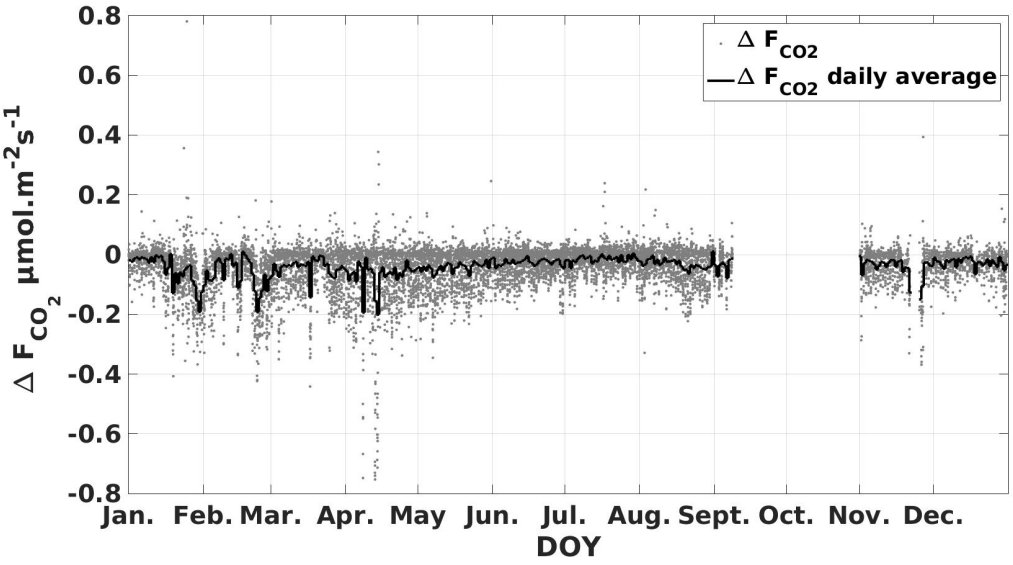

Figure 4.2: Difference between CO_2 flux of this study and CO_2 WPL corrected flux ($\Delta F_{CO_2} = F_{CO_2,this\ study} - F_{CO_2,WPL}$) in $\mu mol.m^{-2}.s^{-1}$ for the year of 2015

4.1.2 Relation between CO_2 fluxes and velocities

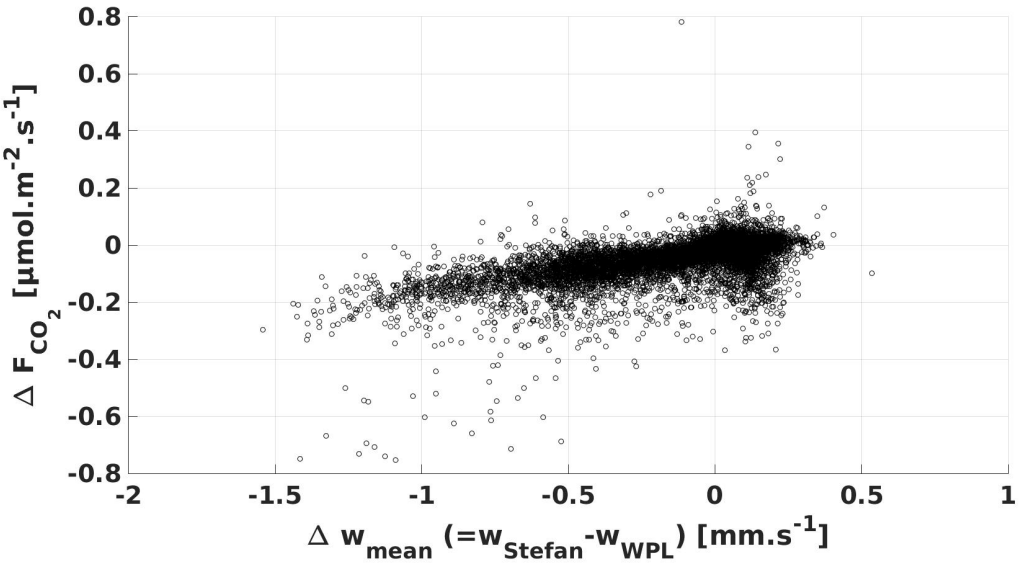

Figure 4.3: Scatter plot of differences of CO_2 fluxes [$\mu mol.m^{-2}.s^{-1}$] versus the differences of mean vertical velocities [$mm.s^{-1}$].

Figure 4.3 represents the dispersion of the differences in CO_2 fluxes versus the differences in the velocities associated ($\widetilde{w} - \overline{w}$). The relation between both appears quite linear, the absolute highest differences of fluxes are found for the highest velocities differences. The maximum of -0.8 $\mu mol.m^{-2}.s^{-1}$ is found in the range of $\Delta w \in [-1.5; -1] mm.s^{-1}$ The slope of the linear relation is approximatively 0.2 $\mu mol.m^{-2}s^{-1}/(mm.s^{-1})$ and this result encouraged the study, in the following sections, of the factors influencing these two velocities.

4.1.3 Relationship with turbulent fluxes

Figure 4.4 presents the scatter plot of ΔF_{CO_2} as functions of the turbulent sensible (H) and latent heat (LE) fluxes, the sum of the turbulent heat fluxes, and the Bowen ratio. Concerning the relation with H, ΔF_{CO_2} decreases quite linearly with a slope of -0.4 to -0.1 $nmol.m^{-2}.s^{-1}/(W.m^{-2})$ with increasing sensible heat flux. Some minimum values, from -0.4 to -0.8 $\mu mol.m^{-2}.s^{-1}$ are observed beyond 150 Wm^{-2}.

Quasi similarly, ΔF_{CO_2} decreases with the increasing of LE but, on the contrary, the minimum values are observed for $LE < 100\ Wm^{-2}$ and the slope of the decrease is smaller than the slope with H and is about -0.01 %. A maximum value of 0.8 $\mu mol.m^{-2}.s^{-1}$ is noticed for LE close to 50 $W.m^{-2}$ whereas the same value is close to 350 Wm^{-2} for H.

To observe more precisely how the turbulent heat fluxes are linked with each other and with the differences of CO_2 fluxes, their sum and the bowen ratio ($\beta = \frac{H}{LE}$) have been plotted. The scattering of the sum with the differences shows that the behavior is a combination of the two fluxes: minimum values are found between 200 and 500 Wm^{-2} and the values of the slopes seem to be between the preceding slopes (-0.01 to -0.04 %).

The relation with Bowen ratio is less evident; it seems that ΔF_{CO_2} decreases for higher values of β, but the minimums (highest absolute differences) values are found in the range of β between 4 and 12.

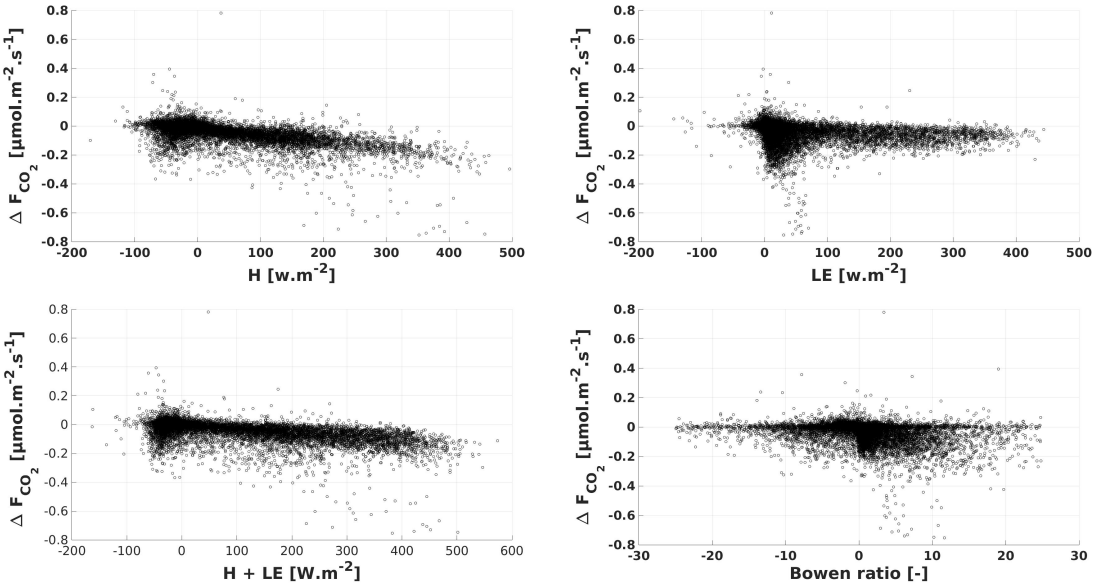

Figure 4.4: Scatter plots of the difference of CO_2 fluxes in $\mu mol.m^{-2}.s^{-1}$ with, at top-left, the turbulent sensible heat flux H in Wm^{-2}; at the top right, the turbulent latent heat flux LE in Wm^{-2}; at the left-bottom, the sum of turbulent heat fluxes $H + LE$ in Wm^{-2}; and at the right-bottom, the bowen ratio β.

4.2 Mean vertical velocity

4.2.1 Evolution over the year

Figures 4.5 and 4.6 present the evolution of the mean vertical velocity at the ground over the year 2015 for this study and for the WPL predictions (respectively, $\widetilde{w}$ and $\overline{w}$). In both figures, half-hours values are represented as well the daily average values. In Fig. 4.5, which represent the mean vertical velocity computed in this study, the half-hours values range from 0 to 60 $\mu m.s^{-1}$ and the daily average ranges from -0.2 to 15 $\mu m.s^{-1}$ from November to May. During the period from May to September, the half-hours values range between 0 to 180 $\mu m.s^{-1}$, the maxima are found in July, and the daily averages oscillate between 15 to 65 $\mu m.s^{-1}$. Note that there are only few negative values and an high concentration of value very close to zero.

The mean vertical velocity derived from WPL theory is represented in Fig.4.6. In this figure, the half-hours values range between -300 to 1500 $\mu m.s^{-1}$. The maximum values are in April and the minimum values are in July. The daily average oscillates from -100 to 500 $\mu m.s^{-1}$ and follows the same periods of half-hour values in terms of extrema.

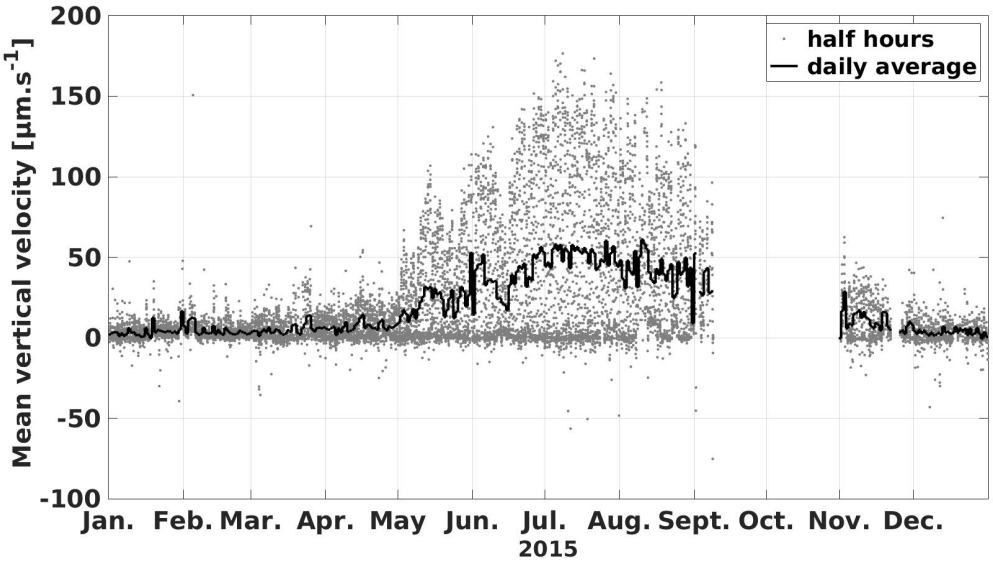

Figure 4.5: Mean vertical velocity in $\mu m.s^{-1}$ from this study. Grey dots represent half-hours values and the black solid line represents daily average values during the year 2015.

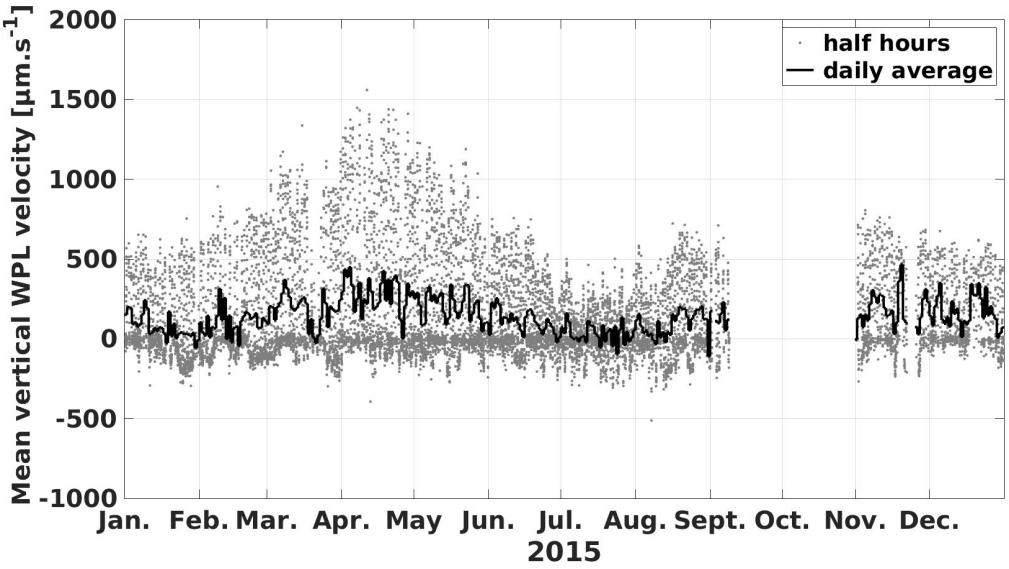

Figure 4.6: Mean vertical wind velocity from WPL theory $\mu m.s^{-1}$. Grey dots represent half-hours values and the black solid line represents daily average values during the year 2015.

4.2.2 Diurnal cycles

In this subsection, the daily cycles of the mean vertical velocity, at the ground, for the WPL theory and for this study have been plotted for 4 months and for the whole year 2015. The 4 months represent one month of each seasons of the years: January for the winter, April for the spring, July for the summer and, since the months of September and October have known material issues, the month of November has been chosen to represent the autumn. For the annual daily cycle, for each half-hour an average is realized over 11526 available values. And with close to 1500 values for the other months, depending on the size of the months and the numbers of "NaN" values detected in the month.

Figure 4.7 represents the daily cycles of this study (eq.2.14). For the 4 months and the annual average, all values are positives from 6 AM to 9 PM and very close to zero during night time, except for the month of July where a value negative of -3 $\mu m.s^{-1}$ is observed. July is the month where mean vertical velocities reach the maximum values of 135 $\mu m.s^{-1}$ at 1 to 2 PM. The month with the minimum values is January which has a velocity of about 10 $\mu m.s^{-1}$ from 10 AM to 3 PM. In November, the maximum velocities are reached at 10H30 AM with a value of 25 $\mu m.s^{-1}$.

Figure 4.8, similar to Figure 4.7, represents the diurnal cycle of the mean vertical velocity at the ground following the eq.2.10 of WPL theory. During night time, from 10 PM to 6 AM, $\overline{w}$ is negative with values close to -25 $\mu m.s^{-1}$. Nevertheless, for the month of July and at the same time that the other Fig.4.7, the mean vertical WPL velocity is positive and close to 10 $\mu m.s^{-1}$. For the four seasons and the annual mean diurnal cycle, the velocities range between -175 to 1000 $\mu m.s^{-1}$. The maximums velocities are observed for the month of April and the minima for the month of July, in contrast to the Stefan velocities computed in this study. During day time, from 6 AM to 9 PM, the annual average WPL velocity is close to 200 $\mu m.s^{-1}$.

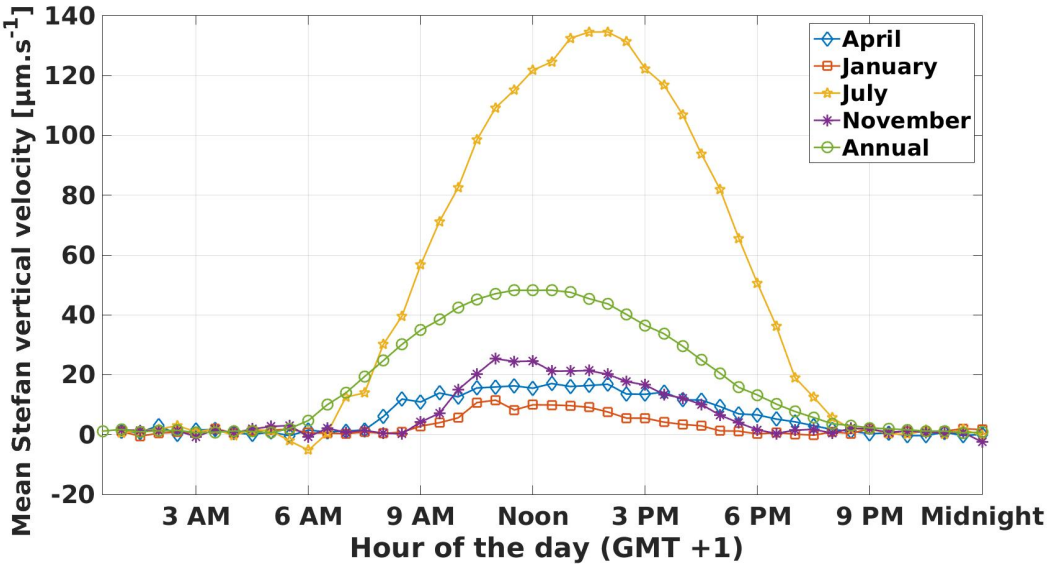

Figure 4.7: Diurnal cycle of mean vertical velocities at the ground in $m.s^{-1}$, for this study, for the month of January (□, red line), April (⋄, blue line), July (empty ⋆, yellow line), November (∗, mauve line) and the annual mean value (∘, green line).

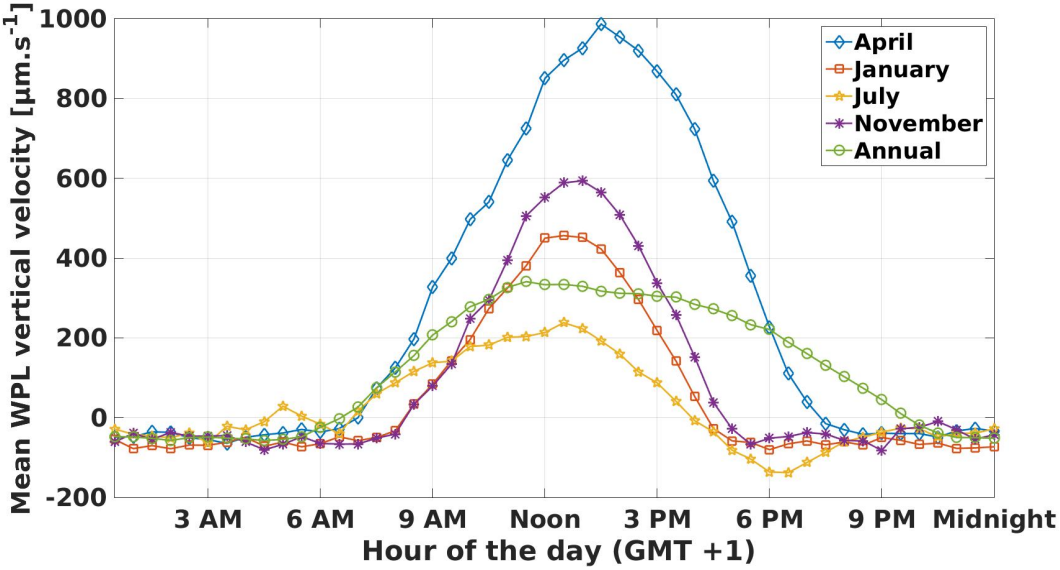

Figure 4.8: Diurnal cycle of mean vertical velocities at the ground, for WPL theory in $m.s^{-1}$, for the month of January (□, red line), April (⋄, blue line), July (empty ⋆, yellow line), November (∗ , mauve line) and the annual mean value (∘, green line).

4.2.3 Influence factors for the mean vertical velocity

To appreciate more easily the influences of parameters influencing the velocities $\widetilde{w}$ and $\overline{w}$, the bowen ratio (fig.4.9 (d)), the sum of turbulent heat fluxes (Fig.4.9 (c)) and the turbulent fluxes (Fig.4.9 (a) and (b)) have been plotted. With the respect to the turbulent latent heat flux, the relationship is forced. For the increasing LE, $\widetilde{w}$ increases with a slope of 500 $nm.s^{-1}/(W.m^{-2})$. In relation to H, the highest values of $\widetilde{w}$ are in the range of $H \in [-100; 100]$ $W.m^{-2}$. The sum of the turbulent fluxes in relation with the mean vertical velocity is not very clear. $\widetilde{w}$ seems to increase with the augmentation of the surface energy but with a large dispersion of values from 0 to 180 $\mu m.s^{-1}$. According to the Bowen ratio, the highest velocities are observed for $\beta \in [-1; 1]$ but the asymmetry of the scattering indicates that velocities between 0 to 50 $\mu m.s^{-1}$ are mainly for $\beta > 0$.

Figures 4.9 (e) and (f) show the relation of the mean vertical WPL velocity ($\overline{w}$) with H and β. Regarding the relationship with H, the relation is linear and follow a ratio of $4\mu m.s^{-1}.W^{-1}.m^{-2}$. Concerning the relationship with β, quasi all value are in range of -10 to 10 of the bowen ratio. The sign of the velocity changes in respect with the bowen ratio: for $\beta < 0$ the velocities are negatives and for $\beta > 0$ the velocities are positives.

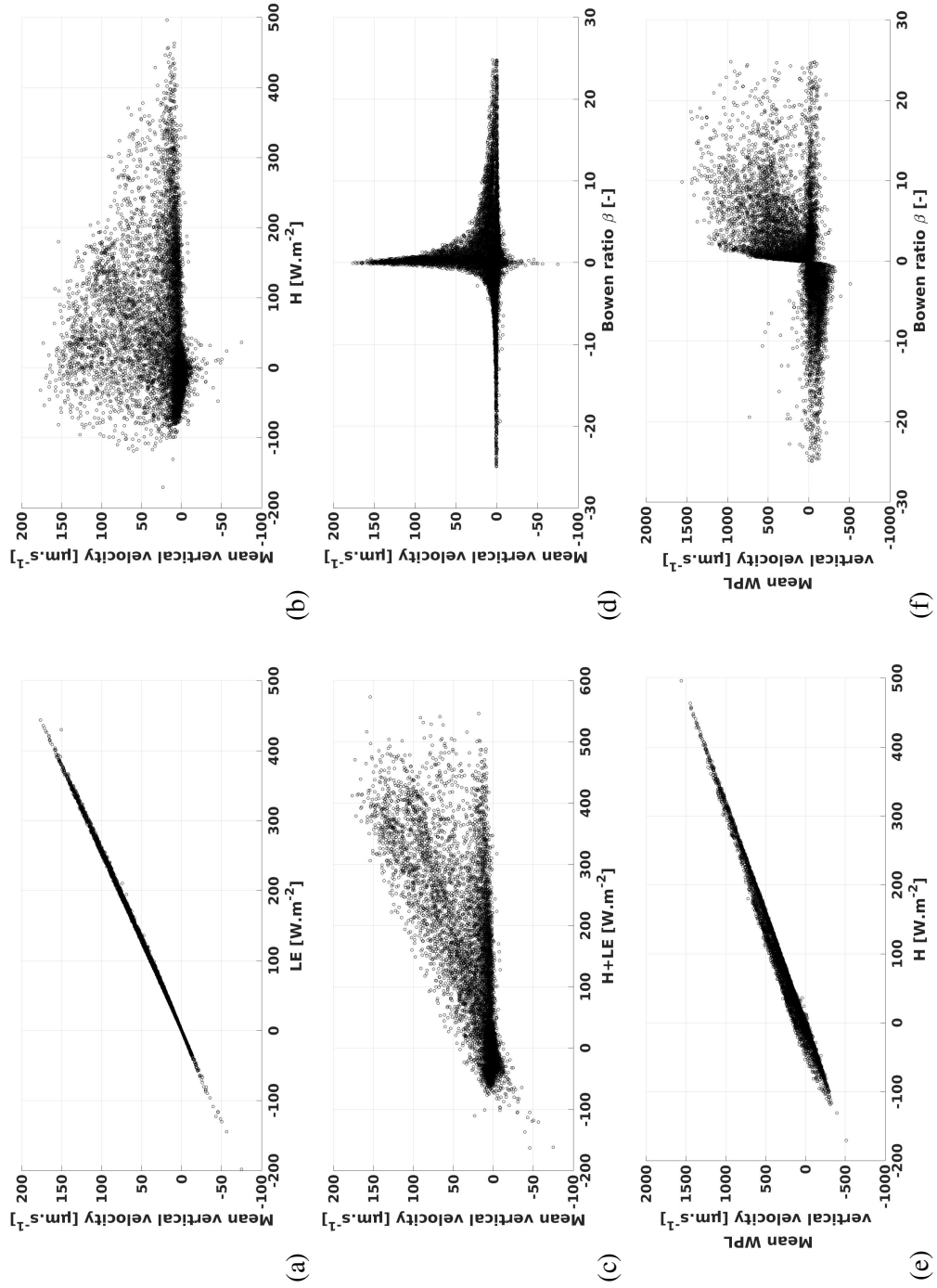

Figure 4.9: Relationship between the mean vertical velocity with: LE in Wm^{-2} (a); H in Wm^{-2} (b) sum of turbulent heat fluxes in Wm^{-2} (c); Bowen ratio (d). And mean vertical WPL velocity for H in Wm^{-2} (e) and Bowen ratio (f) during the whole year of 2015.

Chapter 5

Discussion and conclusion

5.1 Discussion

The aim of this study was to compare two theoretical methods of CO_2 flux computation, using the same filtered data, from an eddy covariance system in the wetland of Padul. The site of Padul has been chosen for its flatness, the homogeneity of the plants and the ground, the high values of fluxes and frequency of windy days . The two methods compared are: i) classical CO_2 WPL corrected flux, which is, when using open path IRGA, the reference for computing carbon dioxide fluxes using mean vertical velocity derived from the ideal gas law; ii) the method of this study, which is derived from molar average velocity and Stefan flow to characterize a non diffusive part added to a diffusive part caused by evaporation. As results, the average difference of these two fluxes is -0.04 $\mu mol.m^{-2}s^{-1}$ (Fig.4.2) and a rate of difference of 0.2 $\mu mol.m^{-2}s^{-1}/(mm.s^{-1})$ (Fig.4.3). These results highlight the fact that one of the two methods overestimate/underestimate the capacity of this wetland as source/sink of carbon dioxide. Indeed, whereas the fact that ΔF_{CO2} ranges in [-0.8;0.2 $\mu mol.m^{-2}s^{-1}$], nearly all values are systematically negative. Since negative values indicate uptake, the results are in accordance with the literature (MEA.2005; Brix et al. 2001).

Considering a surface of 3.5 km^2 of Padul wetland, the 0.04 $\mu mol.m^{-2}s^{-1}/(mm.s^{-1})$ difference of flux leads to a difference of 194 Kg of C02 per year from one computation to the other. It is important to determine which computation represents the most exactly the exchange of CO_2 in Padul's wetland. In the results other parameters were represented to discuss the main factors which can affect these differences, either in fluxes or in mean vertical velocities.

First of all, the order of CO_2 fluxes was controlled by a simulation with Eddy Pro software for the month of July. The proximity of the results (from the script of this study and the reference Eddy pro) indicates that the computation of this study are situated in good range of order.

The main result of interest is the difference between two way of computation in the same script: the current reference, WPL corrected fluxes, and the fluxes of this study. Indeed the differences, in the same script and with exactly same data, allow us to eliminate uncertainties of pre and post-filtering.

The main improvement of this study should to estimate the uncertainties and the errors. The errors can appear due to instrumentation imprecisions; the statistical operations made during computation and for graphic representation; and the approximations made from initial hypothesis. Either for both the mean vertical velocities ($\widetilde{w}$ and $\overline{w}$) and the density of CO_2 trace gas (main parameters of CO_2 fluxes), the results are out of precision measurement instruments ranges. Regarding the statistical operations realized during this work, the very large disparity of data and their distributions underlie approximation that this study does not take into account. For the graphical representation, several average values are represented. These averages can not be interpreted as "absolute" values but rather as an order of value's ranges. In fact, the number of elements av-

eraged is not exactly the same for each period of the year and the extremes, whereas their tiny numbers, influence more the averages than values close to the average. A post filtering of results, in these assumptions, should be considered and in terms of eddy covariance measurements is still an object of many research, (Mauder, 2008; 2013). Concerning the initial assumptions, horizontal homogeneity and perfectly vertical placement of anemometer, some errors are included in results but, for the homogeneity, the large surface of foot print with same kind of ground/plants seems reasonable and should not influence substantially the results. Regarding the vertical placement of anemometer, since a slope of 5 %, which is undoubtedly not the case in Padul site, should not influence more than 0.4 % the vertical wind measurement (correction following a cosine function of the slope α), this error is not considered.

Figure 4.4 shows the influence of turbulent heat fluxes on the difference of dioxide carbon. These relations indicate that the highest differences occur during half-hours with more sensible heat than latent heat. At the same time, it is noticeable that differences of F_{CO2} increase with the sum of $H + LE$, whereas the maximum differences are found for $LE < 10\ W.m^{-2}$. In order to evaluate the determinant factor of the scatter plot of ΔF_{CO2} versus the bowen ratio was represented. The Bowen ratio is very helpful to discuss the relative importance of the turbulent latent heat fluxes. For high values of β, between 5 to 30, H is the dominant turbulent heat flux in front of LE. On the contrary, a bowen ratio close to zero indicates that LE is dominant.

Then, the maxima value of CO_2 fluxes differences appears to be mainly control by positive values of β between 5 to 10. As seen with figure 4.3, the differences are controlled by the differences between the mean vertical velocities (of Stefan, for this study, and of WPL theory) at the ground. These velocities are largely dependent on turbulent heat fluxes (fig. 4.9), and so on, the Bowen ratio.

The diurnal cycles of these velocities has been plotted, in Fig.4.7 and Fig.4.8. The first very important point is the difference of one order of magnitude between the both velocities. From WPL theory, the velocity at the maximum can reach $1.5mm.s^{-1}$ whereas for Stefan velocity the maximum velocity computed was about $0.18mm.s^{-1}$. For the velocity of this study, it is observed that $w_{July} > w_{Annual} > w_{November} > w_{April} > w_{January}$. Note also that only positive values are observed in this diurnal cycle and that depending on the hour of the day, the relation $w_{November} > w_{April}$ can change. The Stefan velocity is derived from evaporation (eq 2.14 and Fig.4.9 (e)) and indicates that turbulent energy is mainly used in July to evaporate water rather than to warm it, as during other seasons. The diurnal cycle of the WPL mean vertical velocity at the surface shows: $w_{April} > w_{November} > w_{January} > w_{Annual} > w_{July}$. Equation 2.9 and Fig. 4.9 (e) and (f) show that the mean velocity derived from WPL theory is driven by the sensible heat flux and/or low values of bowen ratio. Then, on average, April is the month where energy at Padul is mainly used to warm the water (relatively cold after melting in the mountains) and the air above it without use of energy for phase change (liquid $\rightarrow$ water vapor). November is the second month with the highest WPL velocities. This inter-season month comports as the month of April excepting that evaporation is more present at this time. January, as November, is a month which has a low β, certainly lower than November, or both fluxes H and LE are smaller in this period which induces smaller velocities than November. Finally, July is the month which has the minimum velocities. This could come from the fact that β is very low in this season. Therefore, the bowen ratio explains the differences between WPL and Stefan velocity, since that differences in CO_2 fluxes are driven by evaporation (LE) in comparison with H. For high β, in spring, WPL velocities are the largest versus other seasons. The Stefan velocities are largest in summer versus other seasons with low β, due to high evaporation.

In situ observations show that the water table in Padul, during summer time, is very low,(Serrano-Ortiz 2017). Because the water is stagnant at the Padul site, it is considered that water infiltration into the ground and water flowing out of study site explain behaviors of principally evaporative nature to remove water.

In addition, Fig.4.9 (f) shows that for negative β the WPL velocities are negative and positive for $\beta > 0$. Considering that a positive sensible heat flux will, mostly, expand the volume of the air parcel and a negative one will compress it. And by considering an impermeable boundary condition at the ground for an air parcel, a negative value has no physical sense for the vertical wind velocity.

Therefore the velocity derived by WPL theory, well correlated with H (Fig. 4.9 (g)), resembles more the velocity of expansion of a volume rather than a velocity at the ground.

With a similar argument, a velocity caused by evaporation of water in surface layer during day time, and mostly summer season, seems more appropriate to describe the boundary conditions at the surface.

5.2 Conclusion

The aim of this internship was to compare two methods of computing CO_2 fluxes from high frequency measurement. The two fluxes compared are: i) flux derived from Webb et al.1980, because an open path IRGA was used to record gases density; ii) a CO_2 flux derived from Kowalski 2017 where flux is decomposed into a diffusive and non-diffusive part, using weighting factor in average definition. The Padul site was chosen for its: horizontal homogeneity, flatness, high values of H_2O and CO_2 fluxes and for the windy conditions occurring very often.

A Matlab© script was developed to treat the year of 2015 raw data base, the script is free and available on the following link: $http://www.ugr.es/andyk/index\_Research.html$. As a result, with same data and same filtering method, a annual average fluxes difference of -0.4 $\mu mol.m^2.s^{-1}$, corresponding closely to $15 gC.m^{-2}.year^{-1}$, has been observed. Moreover, the difference was associated to be driven by the differences in the mean vertical velocities at the ground at the rate of -0.2 $\mu mol.m^2.s^{-1}/(m.s^{-1})$.

Bibliography

[1] Bird R. B., Stewart W. E., Lightfoot E.N.Transport phenomena. New York: John Wiley and Sons, 2002. 780 p. [Dept. Chem. Eng., Univ.Wisconsin, Madison, WI]. Chapter 17.

[2] Borja Ruiz Reverter. Intercambios de CO_2 y vapor de agua en ecosistemas de alta montaña de matorral mediterráneo. Tesis de doctorado. Departamento de Fisica Aplicada, Universidad de Granada.

[3] Burda G., Anderson D. 2010. A brief practical guide to eddy covariance flux measurements. Principles and workflow examples for scientific and industrial applications. LI-COR Biosciences. 212 pp.

[4] Brix H., Sorrell B. K. and Lorenzen B., 2001. Are Phragmites-dominated wetlands a net source or net sink of greenhouse gases? Elsevier. Aquatic Botany 69 pp 313-324.

[5] EEA report.Annual European Union greenhouse gas inventory 1990–2014 and inventory report. N°15. 2016. Submission to the UNFCCC Secretariat.

[6] Foken Thomas. 2008. THE ENERGY BALANCE CLOSURE PROBLEM: AN OVERVIEW. Ecological Applications, 18(6), pp. 1351-1367, by the Ecological Society of America.

[7] Finnigan J.J., 2009. Response to comment by Dr. A.S Kowalski on "The storage term in eddy flux calculations". Agricultural and Forest Meteorology. 149: 725-729.

[8] Finnigan, J.J., Clement, R., Malhi, Y. et al. 2003. A Re-Evaluation of Long-Term Flux Measurement Techniques Part I: Averaging and Coordinate Rotation. Boundary-Layer Meteorology 107: 1-48.

[9] Hesselberg, T., 1926. Die Gesetze der auseglichenen atmosphärischen Bewegungen. Beitr. Phys. fr. Atmos., 12: 141-160.

[10] IPCC, 2013: Climate Change 2013: The Physical Science Basis. Contribution of Working Groupe I to the Fifth Assesment Report of the Intergovernmental Panel on Climate Change [Stocker, T.F., D. Qin, G.-K Plattner, M. Tignor, S.K Allen, J. Boschung, A. Nauels, Y. Xia, V. Bex and P.M. Midgley (eds.)]. Cambridge University Press, Cambridge, United Kingdom and New York, NY, USA, 1535 pp.

[11] Kowalski S. A., 2012. Exact Averaging of Atmospheric State and Flow Variables. Depertemento de Fisica Aplicada, Universidad de Granada, and Centro Andaluz del medio Ambiente, Granada, Spain. Journal of the Atmospheric Sciences. N° 1750 vol. 69.

[12] Kowalski A. S. and Serrano-Ortiz P., 2007. On the relationship between the eddy eddy covariance, the turbulent flux, and surface exchange for a trace gas such as CO_2. Boundary-Layer Meteorology. N°124, pp 129-141.

[13] Kowalski Andrew S., 2017. The boundary layer condition for the vertical velocity and its interdependence with surface gas exchange. Atmospheric, chemistry and physics.

[14] Kramm G., Dlugi R. and Lenschow D. H., 1995. A re-evaluation of the Webb correction using density weighted averages. Elsevier. Journal of Hydrology. N° 166 pp 283-292.

[15] Lee X. et al. (eds.), 2004. Handbook of Micrometeorology, 7-31. Kluwer Acedemic Publishers in the netherlands.

[16] Leuning Ray., 2007. The correct form of the Webb, Pearman and Leuning equation for eddy fluxes of trace gases in steady and non-steady state, horizontally homogeneous flows. Boundary-Layer Meteorology. N°123, pp 263-267.

[17] Lienhard J. H. IV and Lienhard J. H. V. 2001. A heat transfer textbook. Third edition. 688 pp.

[18] Liu Heping., 2005. An alternative approach for CO_2 flux correction caused by heat and water vapor transfer. Boundary-Layer Meteorology. N°115, pp 151-168.

[19] Mauder M., Cuntz M., Drüe C., Graf A., Rebmann C., Schmid H.P., Schmidt M., Steinbrecher R., 2013. A strategy for quality and uncertainty assessment of long-term eddy-covariance measurements. Elsevier. Agricultural and Forest Meteorology 169 pp 122-135.

[20] Mauder M., Foken T., Clement R., Elbers J. A., Eugster W., Grünwald T., Heusinkveld B. and Kolle O., 2008. Quality control of CarboEurope flux data – Part 2: Inter-comparison of eddy-covariance software. Biogeosciences, 5, 451–462.

[21] MEA. 2005. Millenium-Ecosystem-Assessment. Ecosystems and Human Well-being: Wetlands and Water Synthesis.

[22] Reynolds Osborne., 1895. On the Dynamical Theory of Incompressible Viscous Fluids and the Determination of the Criterion. Phil. Trans. R. Soc. Lond. A. N°186, pp 123-164.

[23] Schmid, H. P. 1994. Source areas for scalars and scalar fluxes. Boundary-Layer Meteorology 67, 293-318 .

[24] Serrano-Ortiz P., Kowalska N., López-Ballesteros A., Sanchez-Cañete E.P., Runkle B.R.K., Kowalski A.S., Urbaniak M., Olejnik J., Chojnicki B.H. 2017. Warmer climates enhance the C sink capacity of reed wetlands. Under review.

[25] Serrano-Ortiz P., Kowalski A.S., Domingo F., Ruiz B., Alados-Arboledas L., 2008. Consequences of Uncertainties in CO_2 Density for Estimating Net Ecosystem CO_2 Exchange by Open-path Eddy Covariance. Boundary-Layer Meteorology 126:209–218.

[26] Stull Roland B., 1988. An introduction to boundary layer meteorology. Kluwer academic publishers. Dordrecht, Boston, London. 666p.

[27] Webb E. K., Pearman G. I. and Leuning R., 1980. Correction of flux measurements for density effects due to heat and water vapor transfer. Quart. J. R. Met. Soc. N°106, pp 85-100.

[28] Wilson K. , Goldstein A. , Falge E. , Aubinet M. , Baldocchi D. , Berbigier P. , Bernhofer C. , Ceulemans R. , Dolman H. , Field C. , Grelle A. , Ibrom A. , Law B.E. , Kowalski A.S. , Meyers T. , Moncrieff J. , Monson R., Oechel W. , Tenhunen J. , Valentini R. , Verma S., 2002. Energy balance closure at FLUXNET sites. Elsevier. Agricultural and Forest Meteorology 113 (2002) 223–243.

Chapter 6

Acknowledgment

Il y a beaucoup de gens que je souhaite remercier, parce que je pense que dire merci avec sincérité est quelque chose d'important et qui me tient beaucoup à cœur. Si je ne peux citer tout le monde dans cette partie, c'est que trop de monde ont contribué à me faire aller au bout de ce mémoire. De plus, je ne suis pas là pour écrire mon autobiographie mais bien pour distribuer quelques remerciements à la volée dans le peu de langues que je connais!

To begin with the scholar's relationship in France, I would like to say thank you to Chantal Staquet, my master's director, and who was also my first advisor in internship and my math's teacher as well during my bachelor. She encouraged me to think the meteorology in mathematical and mechanical way that I didn't know at this time. Even if the last year was really difficult for me, I have learnt a lot of interesting concept and I will, thus, look at the sky with a different point of view.

Then, I would like to thank my friends of the university, Arthur, DaDa, Camille, Victor, Alban,..., Mathilde who wasn't with us this year (Mathilde tu as un peu exagéré là quand même!!), and also the foreigner friends Ali, Nan, Eva,.., and Giannis the happy Greek giant! (Thank you for the good moment guy I hope visit you in Greece!!). Alors MERCI pour ces bons moments les copains de l'école!

He echo mi ultimo trabajo de estudios en España, hace mucho tiempo que queria descubrir este país con su idioma que me encanta. Mi primeros agradecimientos son por Andy Kowalski que me ha aceptado aquí en Granada y en el despertamiento de física aplicada. Gracias por este trabajo que, a pesar de la dificultades, estaba muy incentivo. Gracias también por la paciencia y las explicaciones de física a un "idiota", que no era capaz de hablar sin hacer una mezcla de Ingles y de Español!

Para seguir en el mismo lugar, de la universidad, muchas gracias a toda la gente del equipo de investigación que me ha acogido. Sobre todo Enrique, Ana, Sara, y Pénelope por tu revisión y tu buenos consejos. Muchas gracias a la otra Ana por todos los momentos de salida en Padul, estaba super divertido de salir con el C15 y hacer aventuras con botas de agua! Gracias también por tu punto de visto sobre la ciencia y la vida en general!

Vivir en Granada fue una experiencia increíble en mi vida. De vivir en san Miguel alto, con ti super TiTi, era una ocasión de encontrarte de verdad y vamos a vernos mas frecuentemente en Francia! Gracias a Gemma, José, y mas reciamente, Leire de haber estar tan simpáticos compis de piso! Aquí en Grana, he encontrado amigos de verdad. Sin vuestro amistad, Ninouch', Victor, Nieves, Ema y Felix los días aquí habían estado aburridos! Gracias para todo y espero veros en Francia!

Maintenant j'aimerais remercier les copains de ma maison du Sappey! Parce que clairement sans eux, je ne serai pas le même! Vous m'avez fait découvrir des choses extraordinaire à la mai-

son comme dans la vie et avez également poussé ma réflexion sur de nombreux sujets, et ça c'est stimulant! Parce que vous Lélé, Krikroux, Geutich', Babe, Yani et Matouchka je suis heureux de partager tant de moments avec vous! Alors CIMERRRR pour votre soutient et votre joie de vivre qui m'a accompagné durant tant d'années!

Pour finir avec ces remerciements, je tiens à dire merci merci et encore merci à ma petite famille: mes deux soeurs Leïla et Oriane ainsi qu'à mon Papou et à ma Mamounch'. Même si vous n'avez jamais bien compris ce que j'étudiais et/ou ce que je faisais durant mes stages, vous m'avez toujours soutenu et encouragé! Malgré les difficultés que j'ai pu rencontrer pendant ces années d'études, me savoir curieux et épanouis était, pour vous, suffisant pour me motiver à aller au bout de mes envies. Vous m'avez d'ailleurs encourager pour tout, et ce, pendant toute ma vie. Je vous en remercie tellement et je vous aime très très fort!!

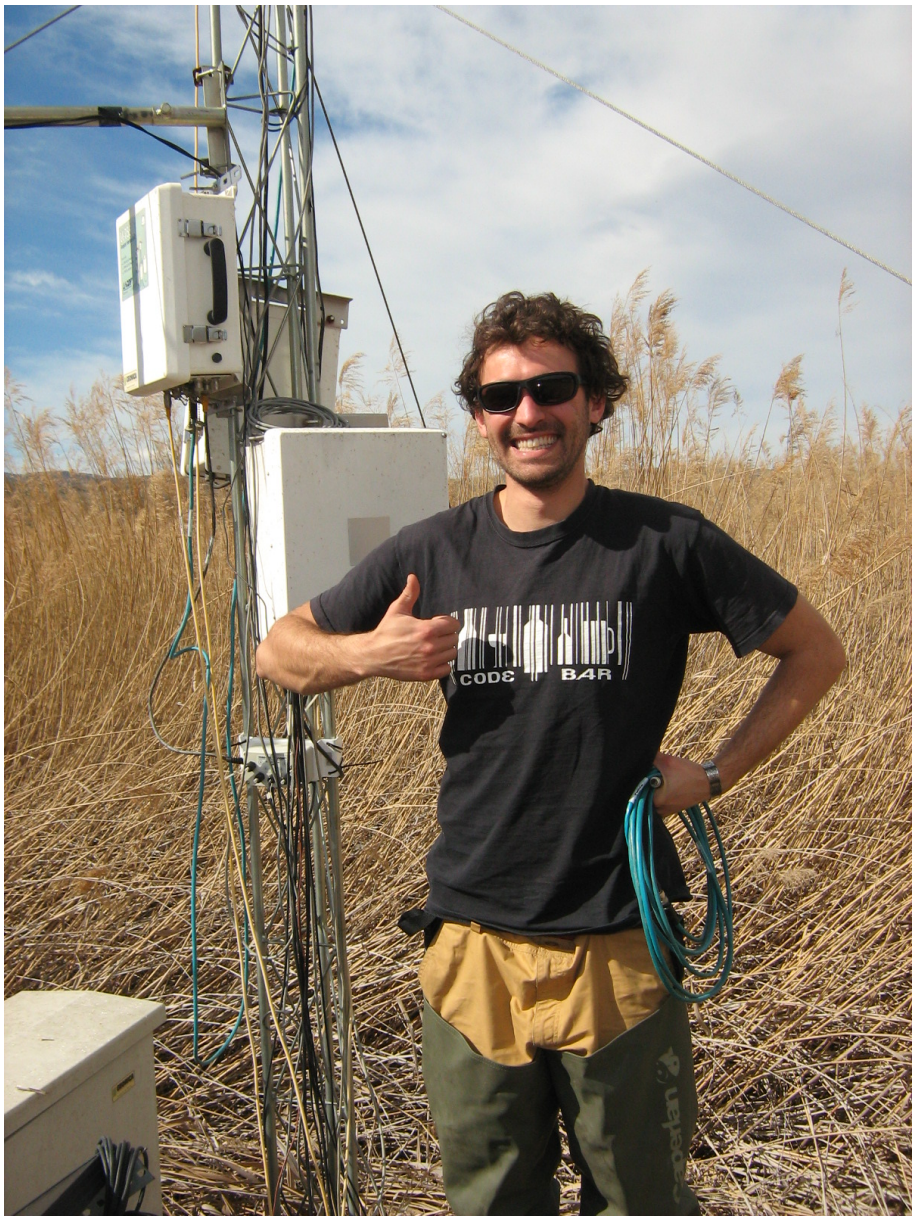

Figure 6.1: Un Gaspi muy muy feliz en la estación de Padul con Ana! "Alors on est pas bien là!"